M.O.Haluschak[1], O.S.Krynytsky[1], D.M.Freik[2]

[1]Ivano-Frankivsk National Technical University of Oil and Gas,
15, Karpatska Str., Ivano-Frankivsk, 76001, Ukraine;
[2]Institute of Physics and Chemistry, Vasyl Stefanyk Precarpathian National University,
57, Shevchenko St., Ivano-Frankivsk, 76018, Ukraine

THERMOELECTRICITY OF SOLID SOLUTIONS
BASED ON LEAD TELLURIDE

A review of works dealing with the problems of obtaining and research on a set of thermoelectric properties of solid solutions based on lead telluride and chalcogenide compounds of other periodic table elements holding good prospects for medium temperature range (500-850) K is made. Chemical compositions, processing factors and temperature ranges whereby the materials have optimal parameters, namely the electric conductivity (σ), the Seebeck coefficient (S), the thermal conductivity (χ), as well as the specific thermoelectric power ($S^2\sigma$), the thermoelectric figure of merit (Z= $S^2\sigma/\chi$) and the dimensionless thermoelectric figure of merit (ZT) are indicated.
Key words: thermoelectric device, periodic steady state, figure of merit, power generation, cooling

Introduction

Possibilities of direct thermal into electric energy conversion have long attracted the attention of researchers and developers of various kinds of equipment. In recent years, thermoelectric effects have found expanding applications. On their basis, thermoelectric generators unique in their parameters have been created that are used in space, under water and in terrestrial (hard-to-reach for service) equipment; generators with nuclear heat sources have been designed. Thermoelectric cooling finds ever-widening application as well. Small overall dimensions, practically unlimited operational life, high reliability of thermoelectric coolers are decisive for their use in instrument making, electronics, medicine and biology [1]. Moreover, in recent years the problem of improving the efficiency of thermal into electric energy conversion has assumed particular prominence due to lack of fossil fuels and considerable discharge to the atmosphere of a large amount of deleterious gases that contaminate the environment, destruct the ozone layer and cause global climate changes [1].

The efficiency of using thermoelectric material is primarily determined by its capability of reaching high values of thermoelectric figure of merit Z ($Z = S^2\sigma/\chi$, where S is the Seebeck coefficient, σ is the electric conductivity, χ is the thermal conductivity) [2].

Most of materials based on IV-VI compounds possess high melting points and combine a set of properties that make them suitable for practical application. Thus, for instance, alloys based on *PbTe*, containing *AgSbTe$_2$*, have high values of $ZT > 1$ both for *n*- and *p*-type [3, 4]. With the advent of modern methods of synthesis and processing, as well as methods for the analysis of microstructure and chemical composition, these materials again became a subject for active studies. The greatest advances in this area have been achieved with the implementation of solid solutions based on *PbTe* with low thermal conductivity coefficients.

This review is an attempt of demonstrating some results of new investigations of *PbTe* based materials.

I. *PbTe-Ag₂Te* system alloys

The composite $(PbTe)_{50-x}(Ag_2Te)_{2x/3}$ with $x = 0, 1, 2, 3$ and 4 (corresponding to *Pb* content 50, 49, 48, 47 and 46 at. %) was obtained as follows [5]. A mixture of *Pb*, *Ag* and *Te* elements of purity 99,999 % or higher was loaded into a quartz ampoule evacuated to $1.33 \cdot 10^{-3}$ Pa and sealed. Then the ampoule was heated to 1273 K (point 1 in Fig. 1) in a vertical programmable tube furnace at a rate of 500 K/h. After holding at this temperature for 6 hours, the ampoule was cooled and then annealed at 973 K (the first annealing, point 2 in Fig. 1) for 2 days with quenching in water. To obtain a homogeneous solid solution, the ampoule was again annealed (second annealing, point 3 in Fig. 1) at 773 K for 3 days.
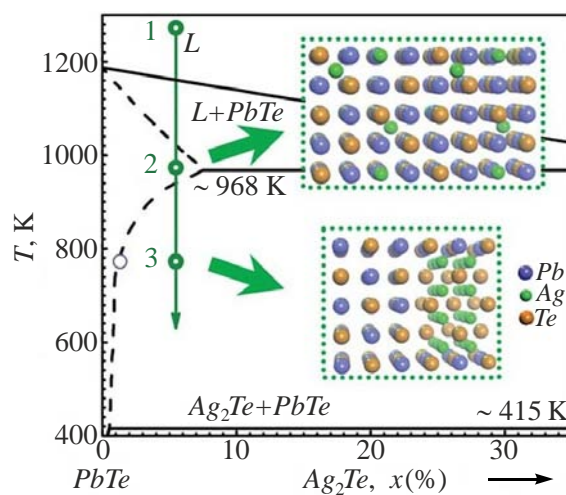
Fig. 1. Phase diagram of PbTe-Ag₂Te system and procedures of thermoelectric material preparation [7].

The resulting ingots were crushed and compacted by hot pressing at 700 K for an hour. The samples thus obtained were used as a source material for doping with *Na* of *PbTe*:*Na*/*Ag₂Te* alloy. The nominal concentration of *Na* corresponded to composition $[(Na_xPbTe_{1+x})_{0.945}(Ag_2Te)_{0.055}]$ with $x = 0...3\%$. The low-temperature annealing results in *Ag₂Te* precipitation in the supersaturated alloy phase. Low thermal conductivity of *PbTe*:*Na*/*Ag₂Te* lattice due to the use of *Ag₂Te* nanoinclusions and excellent electronic properties to complex structure of valence zone result in $ZT > 1.5$ at high temperatures [5]. Moreover, there are considerable improvements of the average value of *ZT* and thermoelectric figure of merit in the entire temperature range, as compared to similar materials without nanostructures and a complex band structure or with small nanostructures.
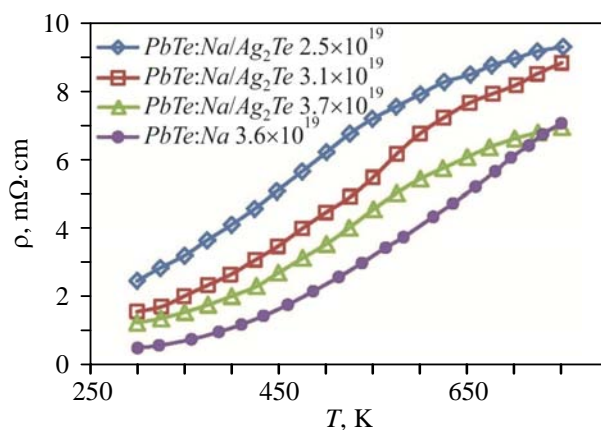
Fig. 2. Temperature dependence of electric resistance for PbTe:Na/Ag2Te and PbTe:Na [5].

The electric resistivity of *PbTe:Na/Ag₂Te* nanocomposites is higher than in *PbTe:Na* (Fig. 2) at low temperatures, when doping levels are almost the same ($p_H = 3.6 \cdot 10^{19}$ cm^{-3} for *PbTe:Na* against $p_H = 3.7 \cdot 10^{19}$ cm^{-3} for *PbTe:Na/Ag₂Te*). Similar to *PbTe:Na* and (*n-PbTe*), the electric resistivity (ρ) grows faster than is commonly expected for a system with a dominant acoustic scattering ($\rho \propto T^{l \sim 1.5}$).

The thermal conductivity (χ) is reduced approximately by 50% in the entire measured temperature range due to *Ag₂Te* nanoinclusions (Fig. 3). The observed reduction of χ is only partly due to the presence of nanoinclusions. The electric conductivity is reduced, hence the electron component of thermal conductivity (χ_E) is reduced, contributing to reduction of χ.
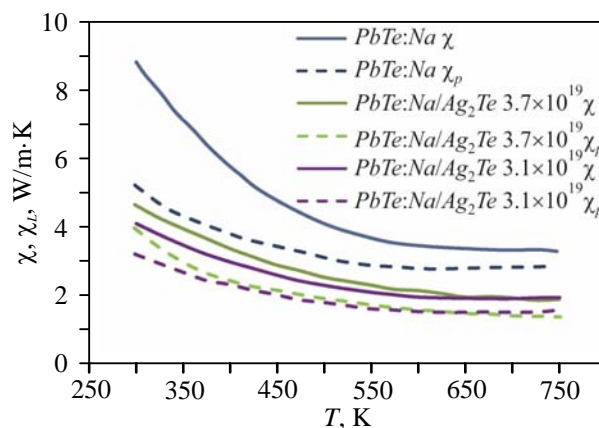
Fig. 3. Temperature dependences of total (χ) and lattice (χ_L) thermal conductivity for PbTe:Na/Ag₂Te alloy as compared to PbTe:Na [7].

II. *PbTe-Sb₂Te₃* solid solutions

In order to obtain *PbTe-Sb₂Te₃* solid solutions based on lead telluride (Fig. 4), at first *PbTe* and *Sb₂Te₃* compounds were synthesized with the use of lead, tellurium and antimony elements that were loaded into evacuated quartz ampoule and placed into a furnace heated to melting point for 1 hour [6,7].
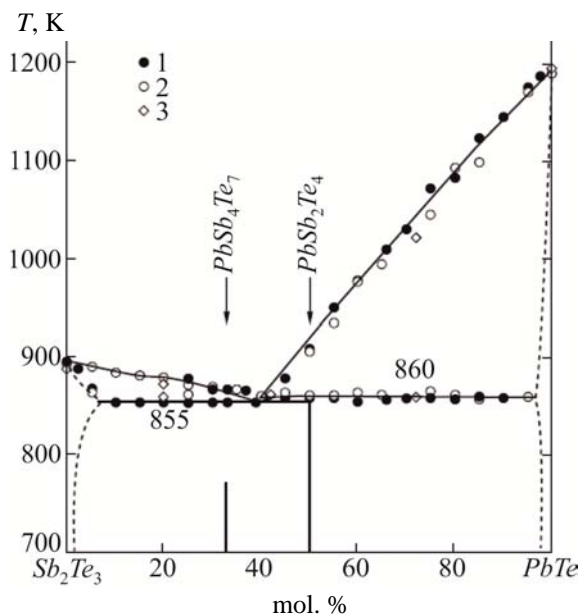
Fig. 4. Phase diagram of PbTe-Sb₂Te₃ system [8].

Following that, the obtained alloys were mixed in proper stoichiometric ratio and loaded into evacuated quartz ampoules that were placed into a furnace and melted at 1250 K for 1 hour with subsequent cooling at a rate of 98 K/h (Fig. 4). The obtained ingots were used for measuring the thermoelectric properties (Fig. 5).
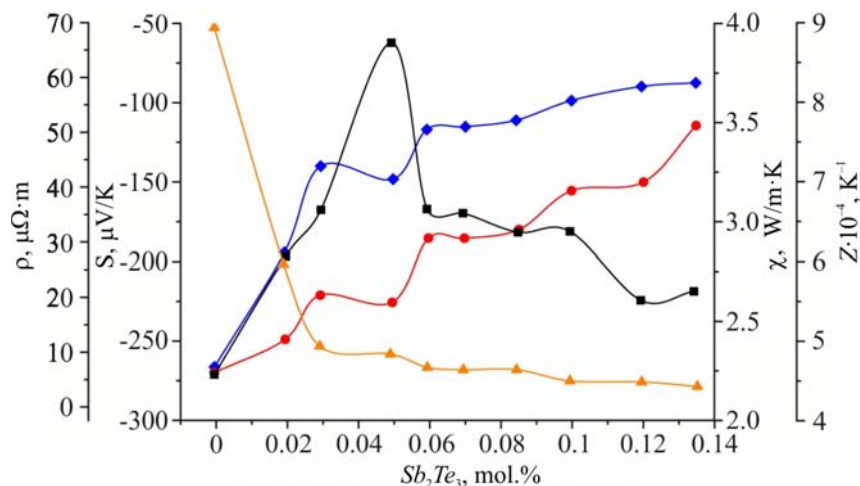
Fig. 5. Dependences of the electric resistivity (ρ – ▲), the Seebeck coefficient (S – ♦), the thermal conductivity (χ – ●), the figure of merit (Z – ■) $(PbTe)_{100-x}(Sb_2Te_3)_x$ on the content of x Sb_2Te_3 [9].

The electric resistivity for *PbTe* as a function of Sb_2Te_3 is first drastically decreased when the amount of Sb_2Te_3 is lower than 0.03 mol. %, and then slowly decreased with increase in Sb_2Te_3 content (Fig. 5 – ▲). The research results show that the type of impact of Sb_2Te_3 as a doping impurity varies due to high pressure and at high temperature [9].

The Seebeck coefficient indicates that all the samples are *n*-type semiconductors (Fig.5 – ♦).

Similar to other doping impurities, total thermal conductivity is increased with increase in Sb_2Te_3 content (Fig. 5 – ●). In so doing, the electron thermal conductivity is increased quickly, and lattice thermal conductivity is continuously reduced with increase in Sb_2Te_3 content for doping with 0.135 mol. % Sb_2Te_3. A reduction in total thermal conductivity as compared to pure *PbTe* is mainly due to a reduction in lattice thermal conductivity, which may be caused by the following factors: atom and ion impurities related to Sb_2Te_3 have a large atomic number which has a greater impact on phonon scattering as compared to other doping impurities; due to effect caused by "softening" of phonons that also reduce lattice thermal conductivity [9].

The thermoelectric figure of merit Z for *PbTe* doped with Sb_2Te_3, calculated from the measured values, is increased and then slowly decreased with increase in Sb_2Te_3 content (Fig.5 – ■). In particular, this figure of merit parameter at room temperature has maximum value ~ 8.7×10^{-4}/K which is about several times higher than in *PbTe* samples doped with *PbI* (2.4×10^{-4}/K) and (2.3×10^{-4}/K) with grain size 0.5 and 0.7 μm, respectively [11].

III. *PbTe-Bi$_2$Te$_3$* solid solutions

To obtain *PbTe-Bi$_2$Te$_3$* solid solutions based on lead telluride, at first *PbTe* and *Bi$_2$Te$_3$* compounds were synthesized from the elements of lead, tellurium and bismuth that were loaded into evacuated quartz ampoule and placed into a furnace heated to melting temperature for 1 hour. Following that, the resulting compounds were mixed in proper stoichiometric ratio and loaded into evacuated quartz ampoules that were placed into furnace and melted at 1250 K for 1 hour with

subsequent cooling at a rate of 98 K/h. The resulting ingots were used for measuring the thermoelectric properties (Fig. 7) [14].
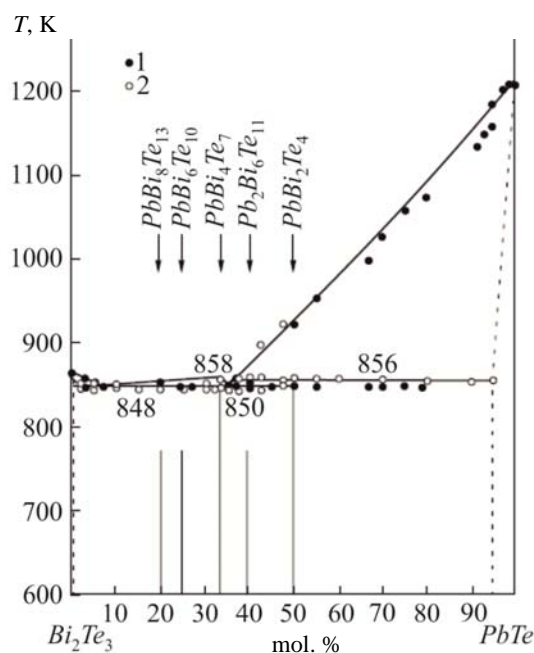
Fig. 6. Phase diagram of PbTe-Bi$_2$Te$_3$ system [8].

For $(PbTe)_{100-x}(Bi_2Te_3)_x$ solid solutions (Fig.7 – ▲) it is seen that the electric resistivity is drastically increased at $x \le 0.3$ and more slowly at $x \ge 0.3$. As compared to the results for Sb_2Te_3 as doping impurity [10], the electric resistivity of $PbTe$ is less sensitive to doping impurity Bi_2Te_3. The difference of electric resistivity from the composition can be due to different ionic radii of these atoms. The ionic radii of Pb, Bi and Sb are 1.26, 1.2 and 1.0 Å, respectively [11]. The difference between the ionic radii of Pb and Sb is greater than between Pb and Bi, so chemical internal stress as a result of Sb substitution for Pb is higher than Bi substitution for Pb with the same concentration of impurity atoms. Moreover, chemical internal stresses should grow with impurity increase.
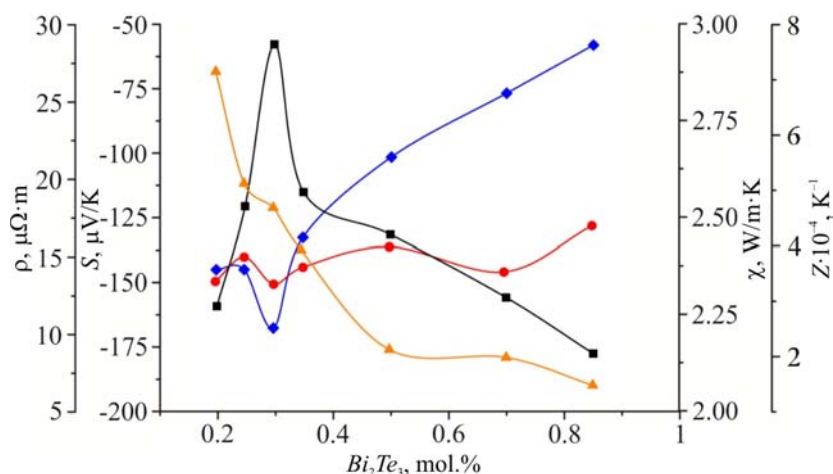
Fig. 7. Dependences of the resistivity (ρ – ▲), the Seebeck coefficient (S – ♦), the thermal conductivity (χ – ●), the figure of merit (Z – ■) (PbTe)$_{100–x}$(Bi$_2$Te$_3$)$_x$ on the content of x Bi$_2$Te$_3$ [14].

From the dependence of the Seebeck coefficient on the content of x (Fig.7 – ♦) it is seen that all $(PbTe)_{100-x}(Bi_2Te_3)_x$ samples have *n*-type conductivity. The Seebeck coefficient in its absolute value is

almost unchanged at $x \leq 0.3$ and has sharp maximum at $x = 0.3$, and then is reduced at $x \geq 0.35$ with increase in x (Fig.7 – ◆). Sharp maxima of the Seebeck coefficient observed for $(PbTe)_{100-x}(Bi_2Te_3)_x$ resemble a behaviour that takes place for metals, intermetallic compounds and heavily doped semiconductors [14]. This is due to the energy dependence on the density of electron states close to the Fermi energy [14].

Total thermal conductivity coefficient χ is retained almost constant and is ~ 2.30 W/K·m (Fig. 7 – ■) which is in agreement with the literature data [15]. Lattice thermal conductivity is linearly reduced, whereas carrier thermal conductivity is linearly increased with increase in x. These results show that thermal conductivity coefficient of $(PbTe)_{100-x}(Bi_2Te_3)_x$, is mainly lattice. Different values of lattice thermal conductivity for *PbTe* doped with Bi_2Te_3 and Sb_2Te_3 also can be due to different ion radii of *Bi* and *Sb* which results in greater crystal lattice deformation and increased phonon scattering. This can be mainly responsible for the fact that lattice thermal conductivity is reduced. Moreover, effect of phonon scattering of heavy impurity atoms should be stronger compared to lighter impurity atoms, so lattice thermal conductivity is much lower than in *PbTe* which is contained in other doping impurities with small grain size [9].

Thermoelectric figure of merit *Z* for $(PbTe)_{100-x}(Bi_2Te_3)_x$ samples at room temperature first is increased and then decreased with increase in x (рис.7 – ■). In particular, at room temperature maximum Z_{max} value is 7.63×10^{-4} K^{-1} which is several fold greater than the literature data for *PbTe* samples doped with PbI_2 with small grain size [9]. The resulting high *Z* value is attributable to considerable Seebeck coefficient and low thermal conductivity. The Seebeck coefficient value 167.2 µV/K at $x = 0.3$ is due to electron topological transition as a result of doping Bi_2Te_3 with high mobility (1212 V·cm^2/s).

IV. *PbTe-PbS* solid solutions

Samples of *PbTe-PbS* system (Fig. 8) with *PbS* content (4, 8, 16, 30, 50 mol. %) were synthesized using *PbTe* and *PbS* as the source materials that were obtained from high-purity elements (*Pb*, *Te* and *S*) whose ratio corresponded to stoichiometric content of *PbTe* and *PbS*. Synthesis took place in evacuated to $1.33 \cdot 10^{-2}$ Pa quartz ampoules at a temperature of 1373 K. The samples were turned over several times in liquid state and cooled to room temperature [16].

PbTe-PbS solid solutions with 8 mol.% *PbS* are unique in that they can be obtained in two forms, namely solid solution and nanostructured material. Fig. 9 shows TEM image of *PbTe-PbS* solid solution (8% mol.% *PbS*) prepared by melt quenching. Single-phase solid solution was then heated to high temperature of two-phase region of pseudo-binary phase diagram [19] where nucleation and
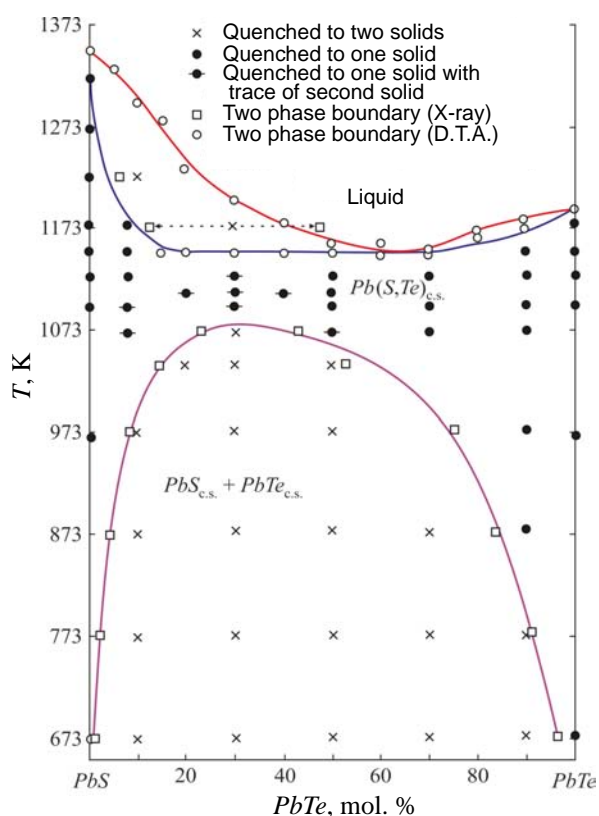
Fig. 8. Phase diagram of PbTe-PbS system [17].

particle growth occurs between 400 K and 500 K. This creates thermodynamically stable nanosize *PbS* particles settling in *PbTe* matrix. At settling of *PbS* nanoparticles, the electron and thermal transport undergo considerable changes [19]. Increase in electron mobility, as well as carrier concentration testify to reduction of electron scattering on the ionized impurities. Formation of thermodynamically stable and sequential *PbS* nanostructures contributes to lattice thermal conductivity decrease by 60% (Fig. 9) [20]. This confirms that nanosize particles in the bulk thermoelectric materials are extremely efficient in reducing lattice thermal conductivity, thus contributing to thermoelectric power increase [20].

In *PbTe-PbS* system, apart from nucleation and growth processes, there is spinodal decomposition which is another ideal mechanism of phonon scattering by nanoparticles on phase boundaries [21]. Hence, the composition and structure, as well as the size and distribution of nanoinclusions, can be controlled due to rational choice of cooling rate and thermal treatment after sysnthesis.

a)

b)

c)
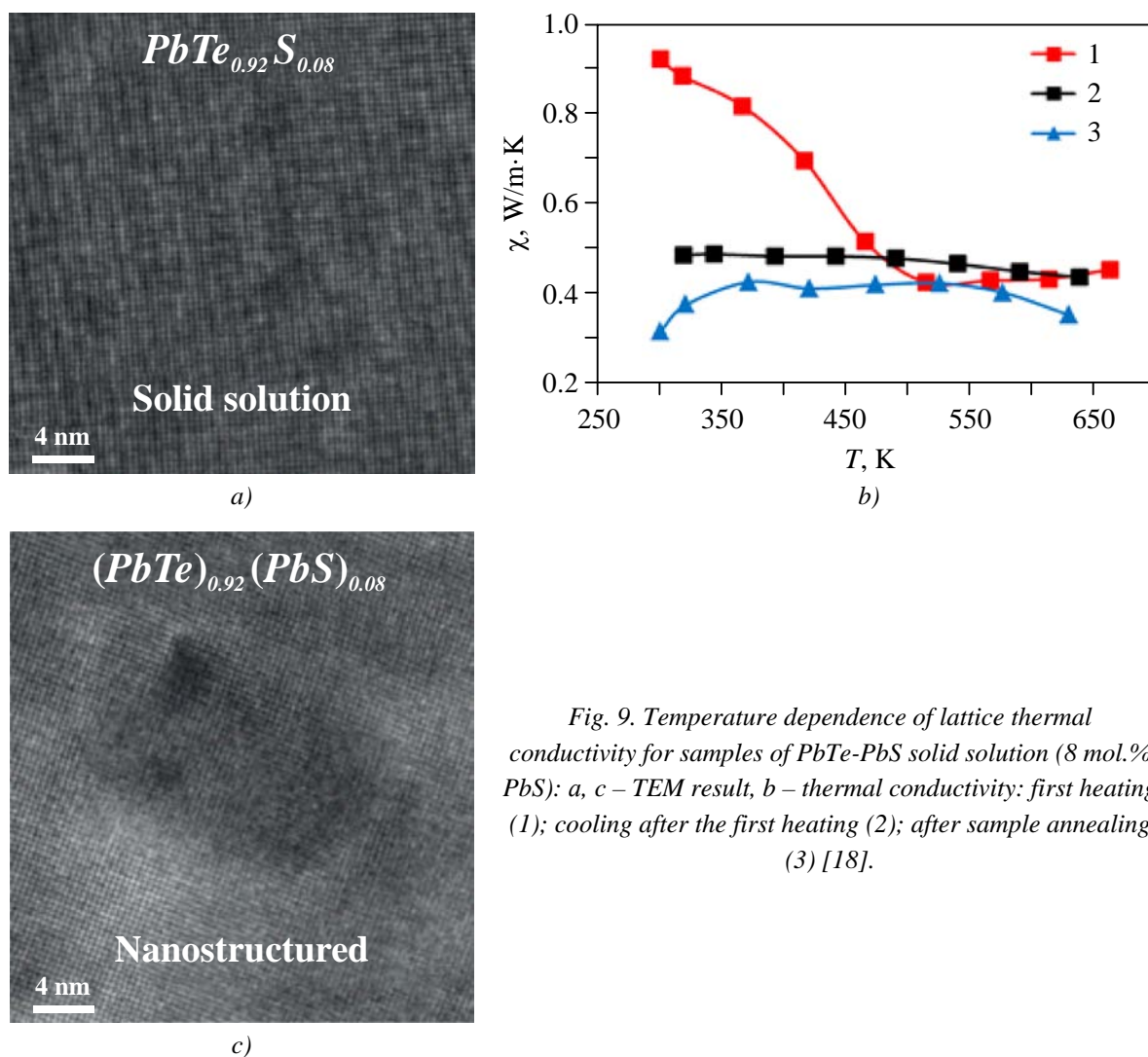
Fig. 9. Temperature dependence of lattice thermal conductivity for samples of PbTe-PbS solid solution (8 mol.% PbS): a, c – TEM result, b – thermal conductivity: first heating (1); cooling after the first heating (2); after sample annealing (3) [18].

Three scale components have been revealed for *PbTe-PbS* system (30 mol.% *PbS*), namely point defects of solid solution (atomic scale), nanoparticles (nanodimensional) and semicoherent phase boundaries with regularly distributed misfit dislocations (Fig. 10) [21].
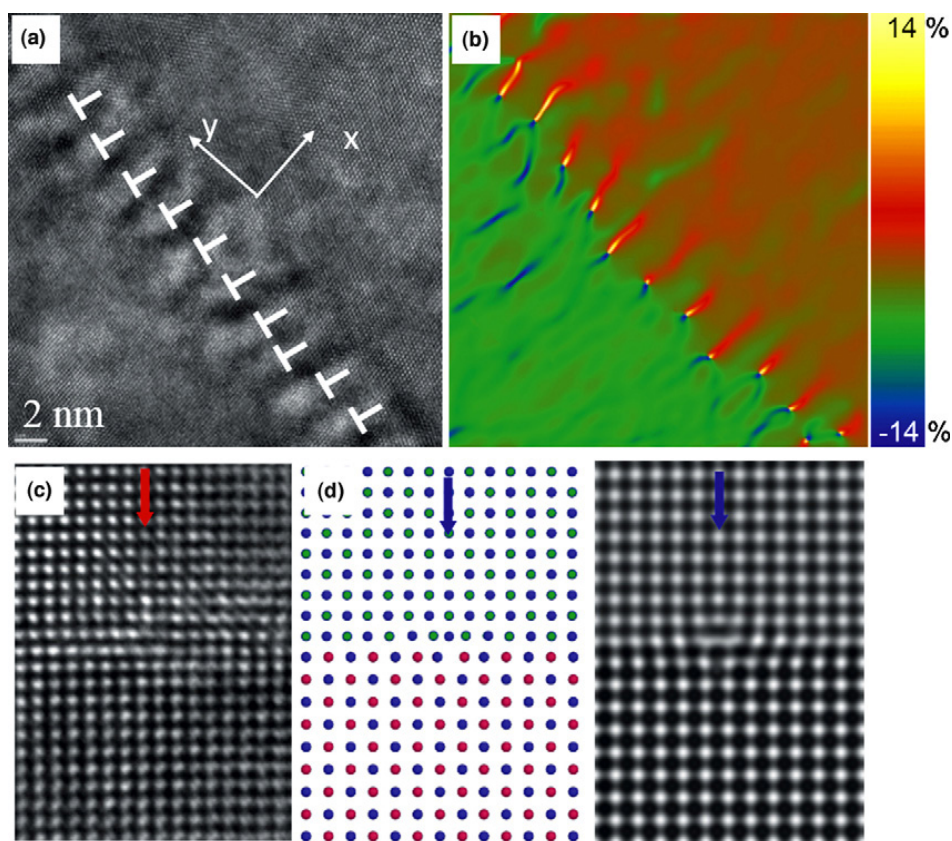
Fig. 10.
(a) – image of lattice of PbTe$_{0.7}$S$_{0.3}$ sample on one Moire fringe boundary;
(b) – image of dislocation centres (high intensity red lines);
(c) – image of lattice including one sharp centre of dislocation with the Burgers vector 1/2 [1 0 0];
(d) – atomic simulation of dislocations between PbTe/PbS [18].

V. *PbTe-PbS* solid solutions doped with *Bi* and *Sb*

Material was prepared from *Pb*, *Bi*, *Te* and *S* (*Pb*, *Sb*, *Te* and *S*) elements with purity 99.99% mixed in a proper molar ratio in quartz tubes and sealed in vacuum $3 \cdot 10^{-3}$ Pa [22]. Later on the samples were heated to 1273 K for 12 hours and quickly cooled to 873 K and held for another 72 hours, following which they were quenched in liquid nitrogen. The samples were made in a ball planetary mill and compacted by spark plasma sintering (SPS) at 853 K for 5 minutes under pressure of 50 MPa.

Thermoelectric properties and figure of merit of *Bi*-doped $(Bi_xPb_{1-x}Te)_{0.88}(PbS)_{0.12}$ samples with $x = 0$, 0.001, 0.003, and 0.005 are shown in Fig. 11. The resistivity of all samples is increased with a rise in temperature over the entire measurement range. As is shown in Fig. 11, *a*, the undoped sample $(PbTe)_{0.88}(PbS)_{0.12}$ has high electric resistivity from $1.98 \cdot 10^{-5}$ Ohm at 300 K and $1.37 \cdot 10^{-4}$ Ohm at 773 K [23]. It is apparently due to intergrain boundary resistance and considerable *PbS* content. Nevertheless, this results in evident increase of the Seebeck coefficient and thermal conductivity reduction. The electric resistance of *Bi*-doped samples is considerably reduced with increase in *Bi* content as compared the undoped sample.

a)

b)

c)

d)
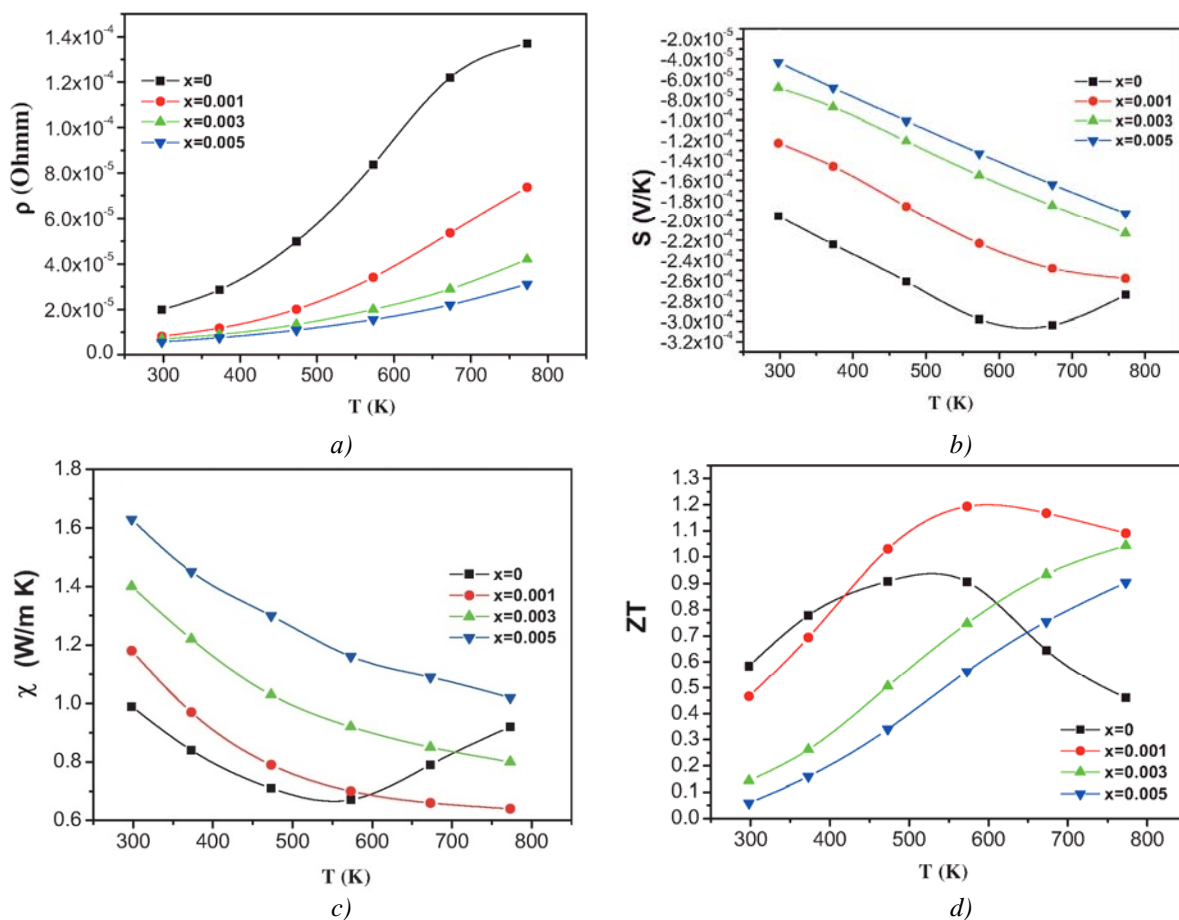
Fig. 11. Temperature dependences of the electric resistivity (ρ – a), the Seebeck coefficient (S – b), total thermal conductivity (χ – c), the value of ZT (d) for doped samples $(Bi_xPb_{1-x}Te)Bi_{0.88}(PbS)_{0.12}$ (x = 0, 0.001, 0.003, 0.005) [22].

The Seebeck coefficients of the investigated solid solutions are negative over the entire temperature range, which indicates to dominant *n*-type carriers (electrons) (Fig. 11, *b*). The absolute values of the Seebeck coefficients for all the samples are increased with a rise in temperature (Fig. 11, *b*).

Total thermal conductivity coefficients for the investigated samples $(Bi_xPb_{1-x}Te)_{0.88}(PbS)_{0.12}$ with x = 0, 0.001, 0.003 and 0.005 are shown in Fig. 11, *c*. Total thermal conductivity for the undoped sample $(PbTe)_{0.88}(PbS)_{0.12}$ is reduced from 0.99 to 0.67 W/m·K with a rise in temperature from 300 to 573 K, and is increased with a rise in temperature in the range of 573 to 773 K (Fig. 11, *c*). Increase in total thermal conductivity at high temperature can be related to increase in lattice thermal conductivity that dominates over total thermal conductivity for the undoped sample. Growing lattice thermal conductivity can be due to anharmonic phonon excitation or partial decomposition of nanostructures at high temperatures.

The figure of merit *ZT* for the investigated samples $(Bi_xPb_{1-x}Te)_{0.88}(PbS)_{0.12}$ with x = 0, 0.001, 0.003 and 0.005 over the entire temperature range is shown in Fig. 11, *d*. Sample $(Bi_xPb_{1-x}Te)_{0.88}(PbS)_{0.12}$ with x = 0.001 shows the highest *ZT* = 1.20 with 573 K, which is much higher than 0.91 for the undoped $(Bi_xPb_{1-x}Te)_{0.88}(PbS)_{0.12}$ at 473 K.

The electrical properties of synthesized and doped samples $(PbTe)_{0.88}(PbS)_{0.12}Sb_xPb_{1-x}Te_{0.88}S_{0.12}$ with x = 0; 0,002; 0,004; 0,006; 0,008 are given in Fig. 12. The resistivity of all samples is increased with a rise in temperature over the entire measured range. The resistivity of undoped sample

$(PbTe)_{0.88}(PbS)_{0.12}$, (Fig. 12, *a*) is rather high and varies from $1.98 \cdot 10^{-5}$ Ohm at 298 K to $1.37 \cdot 10^{-4}$ Ohm at 773 K. This is due to high resistance of intergrain boundaries and high content of *PbS* in a sample prepared by spark-plasma sintering. The resistivity of *Sb*-doped sample is reduced considerably with increase in *Sb* content as compared to undoped sample. Resistivity reduction of *Sb*-doped $(PbTe)_{0.88}(PbS)_{0.12}$ is attributable to substitution of Sb^{3+} ions for Pb^{2+} ions, since *Sb* is an efficient electron donor [24].

a) *b)*

c) *d)*
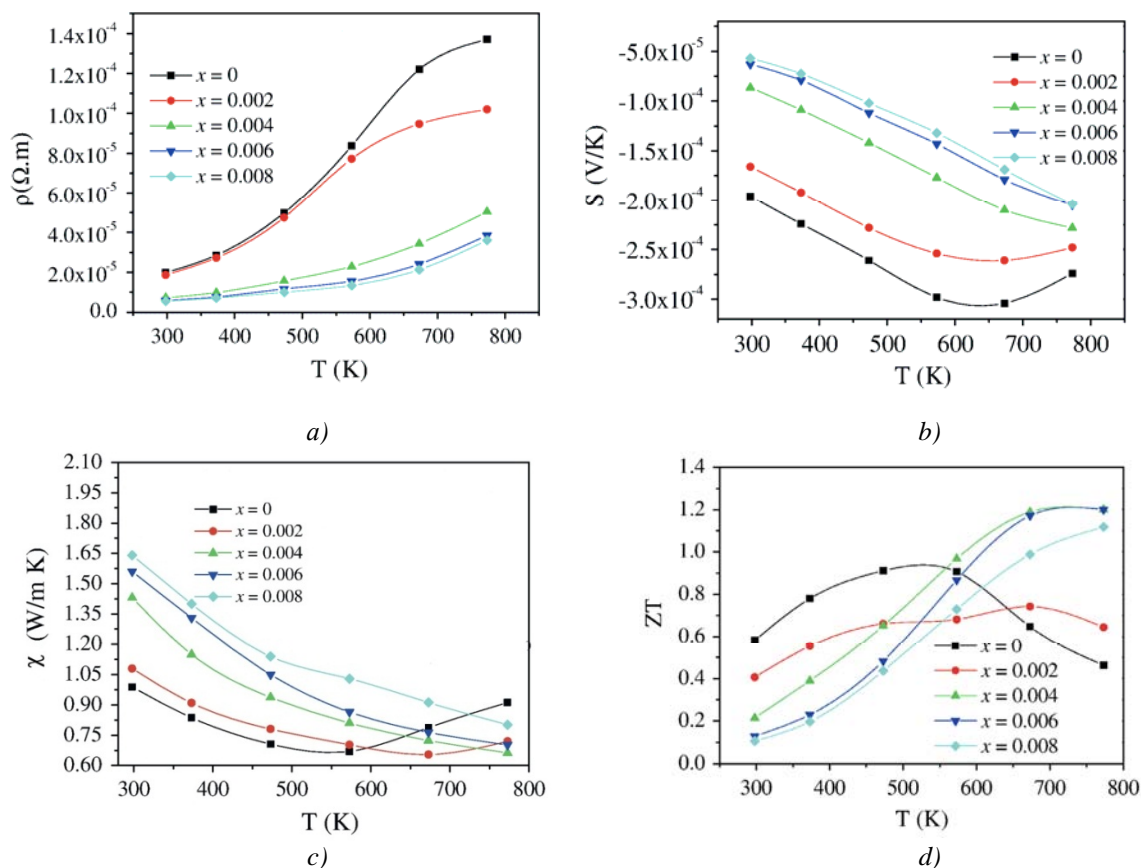
Fig. 12. Temperature dependences of the electric resistivity (ρ - a), the Seebeck coefficient (S - b), thermal conductivity (χ - c), the value of ZT (d) for doped samples $Sb_xPb_{1-x}Te_{0.88}S_{0.12}$ (x = 0, 0.002 0.004, 0.006 and 0.008) [25].

The Seebeck coefficients of investigated samples are represented in Fig. 12, *b*. They are negative over the entire temperature range, pointing to dominant *n*-type carriers (electrons). The absolute Seebeck coefficient for all the samples is increased with a rise in temperature. The absolute Seebeck coefficient for undoped sample $(PbTe)_{0.88}(PbS)_{0.12}$ is linearly increased from 196 µV/K at room temperature to 298 µV/K at 573 K, and then is slightly decreased. For doped *Sb* samples it is decreased with increasing *Sb* content from 196 µV/K with *x* = 0 to 57.0 µV/K with *x* = 0.008 at room temperature.

Total thermal conductivity coefficients for the investigated *Sb*-doped $(PbTe)_{0.88}(PbS)_{0.12}$ samples $Sb_xPb_{1-x}Te_{0.88}S_{0.12}$ with *x* = 0, 0.002, 0.004, 0.006, and 0.008, are shown in Fig. 12, *c*. Total thermal conductivity for the undoped sample $(PbTe)_{0.88}(PbS)_{0.12}$ made by SPS is reduced from 0.99 W/m·K to 0.67 W/m·K with a rise in temperature from 298 K to 573 K, and is slightly increased with a rise in temperature from 573 K to 773 K. Thermal conductivity of $Sb_xPb_{1-x}Te_{0.88}S_{0.12}$ is from 1.08W/m·K to 0.654 W/m·K with *x* = 0.002, from 1.43 W/m·K to 0.663 W/m·K with *x* = 0.004, from 1.56 W/m·K for

0.702 W/m·K, with $x = 0.006$, and from 1.64 W/m·K to 0.802 W/m·K with $x = 0.008$ in the temperature range from 298 K and 773 K. Low thermal conductivity coefficients are attributable to small grain size and grain boundaries that formed as a result of grinding in a ball mill. On doping of $(PbTe)_{0.88}(PbS)_{0.12}$ with Sb, total thermal conductivity is increased mainly due to increase in electron concentration through Sb. The sample of $Sb_xPb_{1-x}Te_{0.88}S_{0.12}$ with $x = 0.004$ shows the highest figure of merit ZT 1.20 at 773 K, which is higher than 0.91 for the undoped $(PbTe)_{0.88}(PbS)_{0.12}$ at 473 K.

VI. *PbTe-PbSe* solid solutions

For *PbTe-PbSe* solid solutions comprising *PbSe* the Seebeck coefficients are lower than for *PbTe*, and the Seebeck coefficient is reduced when molar part of *PbSe* is increased (Fig. 13, *b*) Maximum figure of merit values reach $Z = 2.0 \times 10^{-3}$ K^{-1} which is 30% better than for *PbTe*.

a)   *b)*
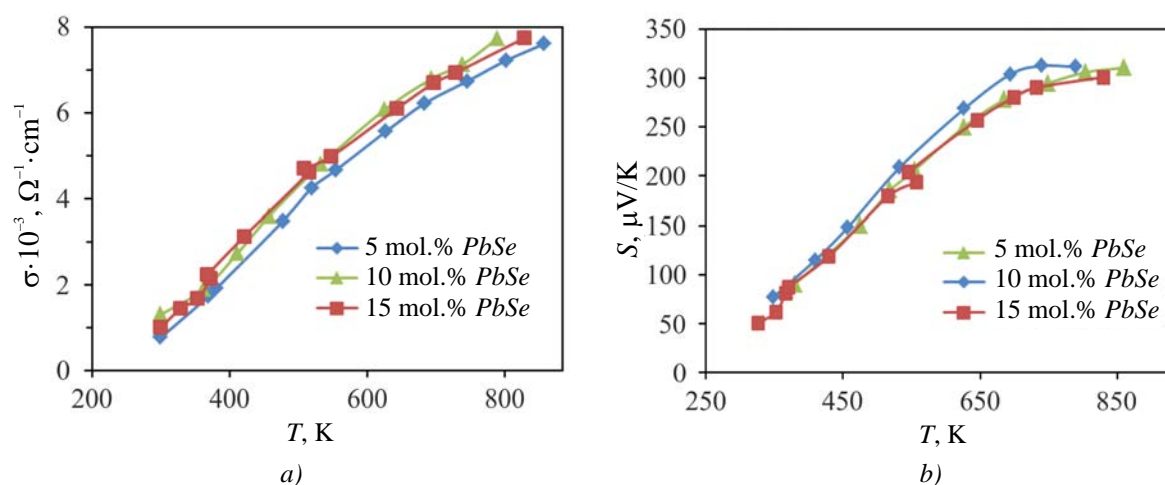
Fig. 13. Temperature dependences of electric conductivity (σ - a),
the Seebeck coefficient (S - b) for p-type PbTe-PbSe [26].

The main contribution to figure of merit enhancement is not related to thermal conductivity reduction, but most probably to higher carrier concentration values at elevated temperatures as compared to *PbTe*. The electric properties, hence the thermoelectric figure of merit, is strongly dependent on carrier concentration. The electric resistivity grows with increase in *PbSe* content. This comes as no surprise, since scattering in this system is known to be considerable [26]. The thermoelectric figure of merit is identical for alloys comprising from 5 to 15 mol% *PbSe*. This is the result of equilibration of two competing processes, namely thermal conductivity reduction and electric resistivity increase. Maximum figure of merit is shown by compounds with *PbSe* content from 5 to 15 mol %.

VII. *PbTe-CaTe* (*BaTe*) systems

Ingots (10 g) of *PbTe-CaTe* [0.5-8 mol.% *CaTe*] doped with Na_2Te (1 mol.%) were synthesized by mixing in proper ratios of high purity source components *Pb*, *Ca*, *Te* and Na_2Te in carbon-coated quartz ampoules. The ampoules were sealed in vacuum $3 \cdot 10^{-3}$ Pa and heated to 1323 K for 15 hours, and then held for 10 hours. Following that, the samples were slowly cooled to 873 K at a rate of 11 K/h and then cooled to room temperature for 15 hours. The test sample of composition $PbTe-Na_2Te$ (1 mol.%) was manufactured by the above procedure in a hermetically sealed ampoule with a similar heating profile.
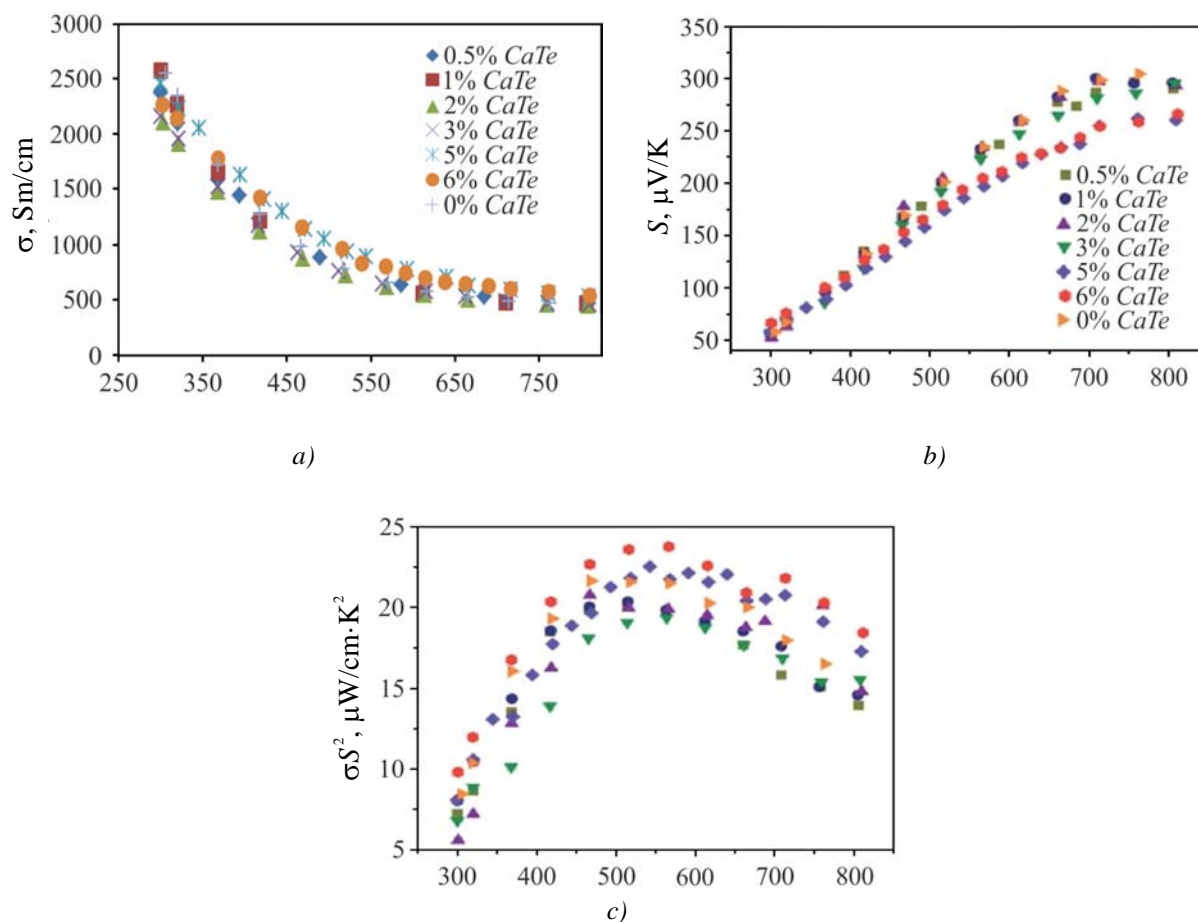
Fig. 14. Temperature dependences of the electric conductivity (σ - a), the Seebeck coefficient (S - b), power factor ($S^2\sigma$ - c) of PbTe-CaTe samples doped with 1 mol.% Na_2Te and PbTe-Na_2Te test sample (1 mol.%) [28].

For all samples of *PbTe-CaTe* doped with 1% Na_2Te, σ is reduced with a rise in temperature, which is indicative of degenerate conductivity for the entire measurement range (300-815 K) (Fig. 14, *a*). As a rule, samples with 6 mol.% *CaTe* had a conductivity from 2240 S·cm^{-1} at room temperature that dropped to 260 S·cm^{-1} at 810 K. Samples including 5 mol.% and 6 mol.% *CaTe* have a higher electric conductivity as compared to others at a higher temperature (450-800 K). The Seebeck coefficients for *PbTe-CaTe* alloys have very similar values, thus, for instance, for *PbTe-CaTe* samples doped with 1 mol.% Na_2Te S = 57 µV K^{-1}, (Fig. 14, *b*). This is consistent with the theory of the contribution of carriers from the zone of heavy holes already at room temperature due to very high *p*-type doping level.

The value of power factor ($S^2\sigma$) of *PbTe-CaTe* samples doped with 1% Na_2Te and the test sample without *CaTe* as a function of temperature is given in Fig. 14, *c*. The highest value of power factor was 10 µW·cm^{-1}·K^{-2} for a sample that comprises 6 mol.% *CaTe* and rises to maximum (24 µW·cm^{-1}·K^{-2}) at a temperature close to 565 K and at 810 K has the value of 19 µW·cm^{-1}·K^{-2}. High values of power factor at high temperatures are observed for 5 mol.% and 6 mol.% *CaTe*. This is attributable to a reduction of hole scattering at high temperatures.
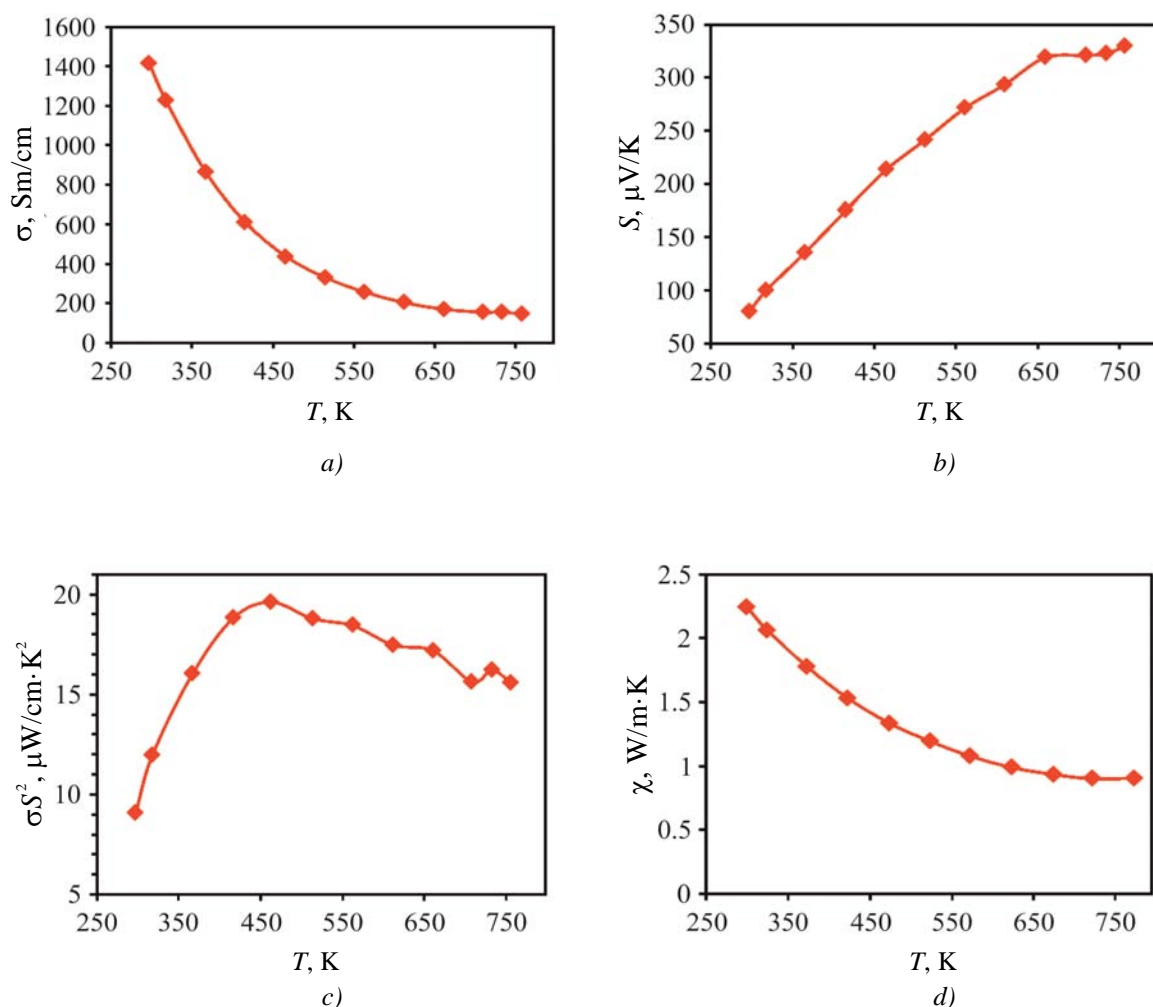
Fig. 15. Temperature dependence of the electric conductivity (σ – a), the Seebeck coefficient (S – b), power factor (S²σ – c) and total thermal conductivity (χ – d) of PbTe-BaTe (3 mol.% BaTe) with the impurity of 1 mol.% Na₂Te [28].

Thermoelectric characteristics of *PbTe-BaTe* alloy (3 mol.%) doped with 1% *Na₂Te* are represented in Fig. 15. The electric conductivity of sample σ = 1410 S·cm⁻¹ at room temperature is reduced to σ = 140 S·cm⁻¹ at 760 K. The value of the Seebeck coefficient measured at room temperature was S = 80 µV·K⁻¹ and is increased to S = 330 µV·K⁻¹ at 760 K (Fig. 15, *b*). The value of power factor at room temperature is 9 µW cm⁻¹ K⁻² and increases to maximum (20 µW·cm⁻¹·K⁻²) at temperature 465 K, and at temperature 760 K it is 16 µW·cm⁻¹·K⁻².

Fig. 16, *a* represents the temperature dependence of total thermal conductivity χ of various samples of *PbTe-CaTe* doped with 1% *Na₂Te* and the test sample. It is clearly seen that introduction of *CaTe* reduces χ. As a rule, at room temperature χ=2.98 W·m⁻¹·K⁻¹ was observed in a sample that comprises 6 mol. % *CaTe* and is reduced to 1.05 W·m⁻¹·K⁻¹ at 825 K.

Fig. 17, *a* represents the temperature dependences of *ZT* for different samples of *PbTe-CaTe* doped with 1 mol. % *Na₂Te* and a test sample that has no *CaTe*. The highest *ZT* 1.5 was achieved at 765 K for the sample with 6 mol.% *CaTe* which is 55% higher than in the test *p*-type *PbTe*. The sample with 5 mol.% *CaTe* also shows high value of *ZT* = 1.45 at 715 K. Samples with the content of (0.5-3) mol.% *CaTe* have *ZT* value in the range from 1.2 to 1.3 at (685-760) K.
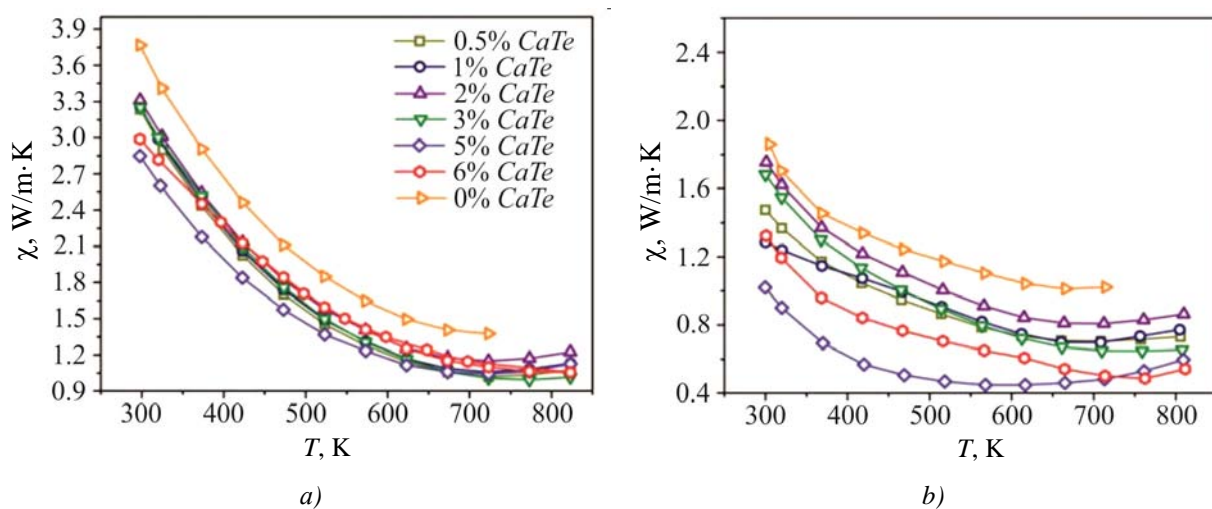
Fig. 16. Temperature dependences of total (χ - a) and lattice thermal conductivity (χ_{lat} - b) of PbTe-CaTe samples doped with 1 mol. % Na$_2$Te and test sample of composition PbTe-Na$_2$Te (1 mol.%) [28].
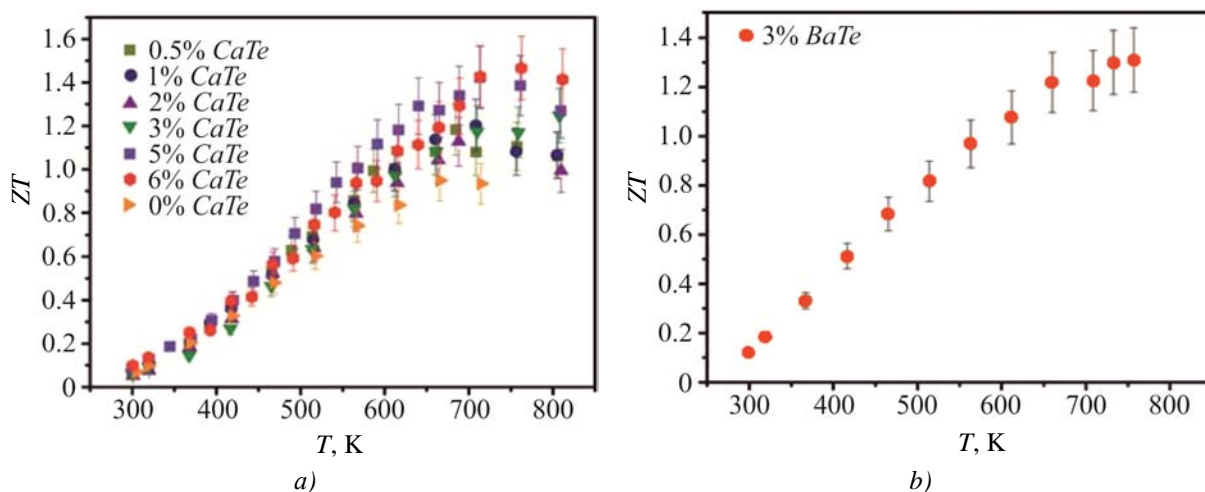
Fig. 17. Temperature dependences of thermoelectric figure of merit (ZT) for (a) PbTe- CaTe samples doped with 1 mol. % Na$_2$Te and (b) PbTe- BaTe (3 mol. % BaTe) doped with 1% Na$_2$Te [28].

With increasing concentration of *CaTe*, *ZT* maximum is displaced from 685 K to 765 K, which is due to higher hole concentration in these samples. For the sample of *PbTe-BaTe* (3 mol.% *BaTe*) doped with *Na$_2$Te* (1 mol.%) *ZT* = 1.3 was achieved at 760 K (Fig. 17, *b*).

Conclusions

1. Characteristics and analysis of the thermoelectric properties of solid solutions obtained on the basis of lead telluride and chalcogenide compounds of other elements of the periodic table are presented.

2. It is established that *PbTe-Ag$_2$Te$_3$* alloys have low lattice thermal conductivity through the presence of *Ag$_2$Te$_3$* nanoinclusions and excellent electronic properties due to complex structure of valence band yielding *ZT* > 1.5 at high temperatures.

3. It is shown that for solid solutions based on *PbTe-Sb$_2$Te$_3$* and *PbTe-Bi$_2$Te$_3$* the thermoelectric properties depend on the content of *Sb$_2$Te$_3$(Bi$_2$Te$_3$)*, and it is established that the optimal content is 0.03 mol.% *Sb$_2$Te$_3$* and 0.3 mol.% *Bi$_2$Te$_3$*, respectively.

4. The *PbTe-PbS* solid solutions with 8 mol.% *PbS* are unique in that they can be obtained in two forms, namely solid solution and nanostructured material which together with spinodal decomposition scatter phonons on phase boundaries and thus reduce the thermal conductivity.

5. In *PbTe-PbSe* solid solutions, the Seebeck coefficients are lower than in pure *PbTe*, and maximum figure of merit values $Z = 2.0 \times 10^{-3}$ K^{-1}, which is possible due to high values of carrier concentration.

6. Samples of *PbTe-CaTe* (*BaTe*) systems with the content of 5 mol.% *CaTe* show high value of $ZT = 1.45$ at 715 K, and samples with 3 mol.% *BaTe* have the value of $ZT = 1.3$ at 760K.

References

1. L.E. Bell, Cooling, Heating, Generating Power, and Recovering Waste Heat with Thermoelectric Systems, *Science* **321**(5895), 1457 (2008).

2. V.M. Shperun, D.M. Freik, and R.I. Zapukhlyak, *Thermoelectricity of Lead Telluride and its Analogs* (Ivano-Frankivsk: Plai, 2000), 250 p.

3. J.P. Heremans, V. Jovovic, E.S. Toberer, A. Saramat, K. Kurosaki, A. Charoenphakdee, S. Yamanaka, and G.J. Snyder, Enhancement of Thermoelectric Efficiency in *PbTe* by Distortion of the Electronic Density of States, *Science* **321**(5888), 554 (2008).

4. K.F. Hsu, S. Loo, Fu Guo, W. Chen, J.S. Dyck, C. Uher, T. Hogan, E.K. Polychroniadis, and M.G. Kanatzidis, Cubic $AgPb_mSbTe_{2+m}$: Bulk Thermoelectric Materials with High Figure of Merit, *Science* **303**(5659), 818 (2004).

5. Y. Pei, N.A. Heinz, A. LaLonde, and G.J. Snyder, Combination of Large Nanostructures and Complex Band Structure for High Performance Thermoelectric Lead Telluride, *Energy Environ. Sci.* **4**, 3640–3645 (2011).

6. O.G. Karpinskii, L.E. Shelimova, E.S. Avilov, M.A. Kretova, and V.S. Zemskov, X-ray Diffraction Study of Mixed-Layer Compounds in the $PbTe\text{-}Bi_2Te_3$ System, *Inorganic Materials* **38**(1), 17–24 (2002).

7. T. Sua, P. Zhua, H. Maa, G. Rend, J. Guoa, Y. Imai, and X. Jia, Electrical Transport and Thermoelectric Properties of *PbTe* Doped with Sb_2Te_3 Prepared by High-Pressure and High-Temperature, *J. Alloys and Compounds* **422**, 328–331 (2006).

8. N.V. Chandra Shekar, D.A. Polvani, J.F. Meng, and J.V. Badding, Improved Thermoelectric Properties due to Electronic Topological Transition under High Pressure, *Physica B* **358**, 14–18 (2005).

9. K.Kishimoto, K.Yamamoto, and T.Koyanagi, Influences of Potential Barrier Scattering on the Thermoelectric Properties of Sintered n-Type PbTe with a Small Grain Size, *Jpn. J. Appl. Phys.* **42**, 501–508 (2003).

10. P.W. Zhu, Y. Imai, Y. Isoda, Y. Shinohara, X. P.Jia, and G.T. Zou, *Mater. Transact.* **46**, 1810–1813 (2005).

11. G.B. Bokii, *Crystal Chemistry* (Nauka: Moscow, 1971), 139 p.

12. P. Zhua, Y. Imai, Y. Isoda, Y. Shinohara, X. Jia, and G. Zou, Composition Dependent Thermoelectric Properties of *PbTe* Doped with Bi_2Te_3, *J. Alloys and Compounds* **420**, 233–236 (2006).

13. E.S. Itskevich, L.M. Kashirskaya, and V.F. Kraidenov, Anomalies in the Low-Temperature Thermoelectric Power of *p-Bi₂Te₃* and *Te* Associated with Topological Electronic Transitions under Pressure, *Semiconductors* **31**, 276–278 (1997).

14. Y.M. Blanter, M.I. Kaganov, A.V. Pantsulaya, and A.A. Varlamov, The Theory of Electronic Topological Transitions, *Phys. Rep.* **245**, 160–257 (1994).

15. S.N. Girard, K. Schmidt-Rohr, T.C. Chasapis, E. Hatzikraniotis, B. Njegic, E.M. Levin, A. Rawal, K.M. Paraskevopoulos, and M.G. Kanatzidis, Analysis of Phase Separation in High Performance *PbTe-PbS* Thermoelectric Materials, *Adv. Funct. Mater.* **23**(6), 747–757 (2013).

16. M.S. Darrow, W.B. White, and R. Roy, Micro-Indentation Hardness Variation as a Function of Composition for Polycrystalline Solutions in the Systems *PbS*/*PbTe*, *PbSe*/*PbTe*, and *PbS*/*PbSe*, *J. Materials Science* **4**, 313-319 (1969).

17. J. He, M.G. Kanatzidis, and V.P. Dravid, High Performance Bulk Thermoelectrics via a Panoscopic Approach, *Materials Today* **16**(5), 166-176 (2013).

18. S.N. Girard, J. He, C. Li, S. Moses, G. Wang, C. Uher, V.P. Dravid, and M.G. Kanatzidis, In Situ Nanostructure Generation and Evolution within a Bulk Thermoelectric Material to Reduce Lattice Thermal Conductivity, *Nano Lett.* **10**(8), 2825 (2010).

19. J. He, S.N. Girard, M.G. Kanatzidis, and V.P. Dravid, Microstructure-Lattice Thermal Conductivity Correlation in Nanostructured $PbTe_{0.7}S_{0.3}$ Thermoelectric Materials, *Adv. Funct. Mater.* **20**(5), 764 (2010).

20. X.X. Li, J.Q. Li, F.S. Liu, W.Q. Ao, H.T. Li, and L.C. Pan, Enhanced Thermoelectric Properties of $(PbTe)_{0.88}(PbS)_{0.12}$ Composites by Bi Doping, *J.Alloys and Compounds* **547**, 86–90 (2013).

21. J. Androulakis, C.H. Lin, H.J. Kong, C. Uher, C.I. Wu, T. Hogan, B.A. Cook, T. Caillat, K.M. Paraskevopoulos, and M.G. Kanatzidis, Spinodal Decomposition and Nucleation and Growth as a Means to Bulk Nanostructured Thermoelectrics: Enhanced Performance in $Pb_{1-x}Sn_xTe$-PbS, *J. Am. Chem. Soc.* **129**, 9780–9788 (2007).

22. W. Liu, X.F. Tang, H. Li, K. Yin, J. Sharp, X.Y. Zhou, and C. Uher, Enhanced Thermoelectric Properties of *n*-type $Mg_{2.16}(Si_{0.4}Sn_{0.6})_{1-y}Sb_y$ due to Nano-Sized *Sn*-rich Precipitates and an Optimized Electron Concentration, *J. Mater. Chem.* **22**, 13653 (2012).

23. J.Q. Li, X.X. Li, F.S. Liu, W.Q. Ao, and H.T. Li, Enhanced Thermoelectric Properties of $(PbTe)_{0.88}(PbS)_{0.12}$ Composites by *Sb* Doping, J. *Electronic Materials*, **42**(3), 2013.

24. I. Kudman, Thermoelectric Properties of *p*-type *PbTe-PbSe* Alloys, *J. Materials Science* **7**, 1027-1029 (1972).

25. D.L. Partin, C.M. Thrush, and B.M. Clemens, Lead Strontium Telluride and Lead Barium Telluride Grown by Molecular-Beam Epitaxy, *J.Vac.Sci.Technol.* **B 5**, 686 (1987).

26. K. Biswas, J. He, G. Wang, S.-H. Lo, C. Uher, V.P. Dravid, and M.G. Kanatzidis, High Thermoelectric Figure of Merit in Nanostructured *p*-type *PbTe-MTe* (*M = Ca*, *Ba*), *Energy Environ. Sci.* **4,** 4675–4684 (2011).